Nuclear Instruments and Methods in Physics Research 225 (1984) 145–152
North-Holland, Amsterdam

MATHEMATICAL MODELLING OF THE PERFORMANCE OF A MWPC

R. BELLAZZINI, A. BREZ, A. DEL GUERRA, M.M. MASSAI and M.R. TORQUATI

Dipartimento di Fisica dell'Università di Pisa, Piazza Torricelli 2, I-56100 Pisa, Italy
and Istituto Nazionale di Fisica Nucleare, Sezione di Pisa, Via Vecchia Livornese, S. Piero a Grado, I-56010 Pisa, Italy

Received 4 January 1984

We have implemented the Erskine formalism for signal development to study in detail the main operational characteristics of a MWPC with a cathode read-out, for both point-like and extenced ionization tracks. A parametrization has been made of the width of the cathode charge distribution and of the ratio of cathode charge over total avalanche charge to be applied for a general class of MWPCs. The integral and the differential nonlinearity of position measurements based on the calculation of the centroid of the cathode signals has been studied as a function of the width of the cathode read-out strips. Left–right and top–bottom assignment capability and interpolation between anode wires has been modelled. The possibility of measuring the angle of incidence of an ionizing particle with a delay-line cathode read-out is suggested.

1. Introduction

In a recent paper [1], Erskine has proposed an algorithm for a numerical solution of the system of linear equations governing the time course of the charge and current induced on the MWPC electrodes by a point source of positive ions, with delta, Gaussian or uniform angular distribution drifting toward the cathodes along the field lines. We have implemented and further developed this algorithm to include extended and inclined ionization tracks and we have utilized the results to model several operational characteristics of a MWPC with cathode read-out.

By means of this modelling it is possible to pose on a sound basis the criteria of choice of many critical parameters of a MWPC, such as anode–cathode gap, spacing between anode wires and number of sampling cathode strips. The particular choice of these parameters determines many important aspects of the behaviour of a MWPC, such as the maximum achievable S/N, the width of the distribution of induced cathode signals, the complexity and number of channels of the associated electronics, etc. Furthermore, several experimental findings in the operation of a MWPC such as the resolution of the left–right or top–botton ambiguity and the interpolation between anode wires can now find a fully quantitative explanation in the framework of this mathematical model.

Whenever possible, or useful, relations were derived in a parametric form to be used with the whole class of MWPCs. A good agreement between the predictions of the model and experimental results was, generally, found. The extension of the model to minimum ionizing particles permitted us to study the time behaviour (rise-time, arrival time of individual ionization clusters) of the corresponding charge and current signals. Finally, the possibility of a measurement of the particle incidence angle is suggested. This can be achieved by means of a simple delay-line cathode read-out.

2. The spatial distribution and the total charge on the cathode

First of all, we have calculated the spatial distribution of the charge induced on the wires adjacent to the avalanche wire as well as that of the charge induced on the cathode wires (or strips) parallel to the anode wires. This calculation can be done for each time, from the avalanche time to the time of collection of the positive ions on the cathodes. In fact, one often needs to know these distributions at early times, for example in fast timing applications, while, in other cases, such as in direct centroid calculation, the knowledge of these distributions after a few microseconds is more important. Fig. 1 shows an example of the cathode distributions as calculated at avalanche time, after 100 ns and after 1 μs for a MWPC whith an anode–cathode gap (d) of 4 mm, a spacing between anode wires (s) of 2 mm and a width of the read-out cathode strips (w) of 2 mm.

The overall charge on each cathode strip is due to the sum of two different contributions: (1) a negative charge induced by the positive ion cloud that is drifting toward the cathode and (2) a positive charge induced by the negative charge distributed on the anode wires. The Erskine formalism takes into account both of these

0167-5087/84/$03.00

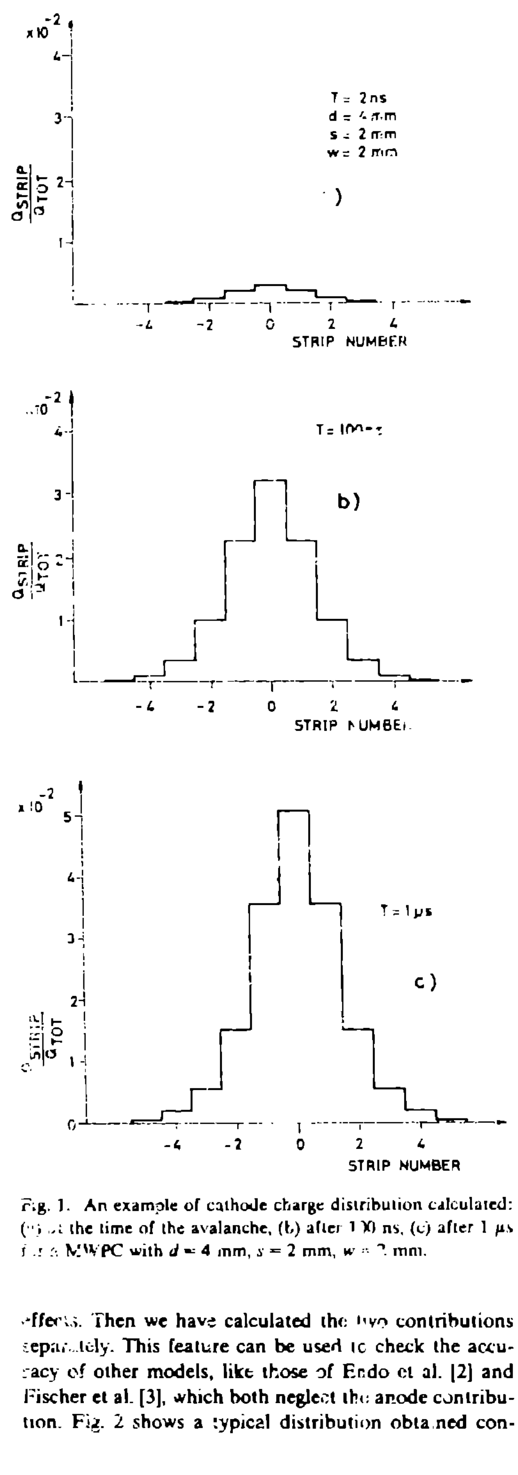

Fig. 1. An example of cathode charge distribution calculated: (a) at the time of the avalanche, (b) after 100 ns, (c) after 1 μs for a MWPC with $d = 4$ mm, $s = 2$ mm, $w = 2$ mm.

effects. Then we have calculated the two contributions separately. This feature can be used to check the accuracy of other models, like those of Endo et al. [2] and Fischer et al. [3], which both neglect the anode contribution. Fig. 2 shows a typical distribution obtained con-

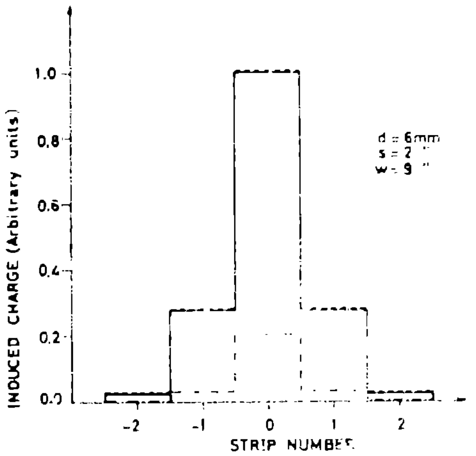

Fig. 2. Dash-dotted line: a typical cathode distribution which takes into account the anode contribution for $d = 6$ mm, $s = 2$ mm, $w = 9$ mm; full line: the corresponding distribution with the anode contribution removed; dashed line: the distribution obtained by applying the Endo model.

sidering both contributions, together with the distribution obtained from the same data, with the anode contribution removed. The two distributions differ in an appreciable way; more significantly, the distribution obtained neglecting the anode plane corresponds, almost exactly, to that obtained applying the Endo model.

The knowledge of the width (fwhm) of the spatial distribution of the cathode signals is important in the design of a MWPC because it is related to the number of channels that are needed to sample the distribution. We calculated this width in a parametric form with the anode–cathode gap and the spacing between anode wires selected as parameters (fig. 3). We have obtained a linear dependence on d and a weak exponential dependence on s: $\mathrm{fwhm}(d,s) = a_1 d\, e^{a_2 s}$ with $a_1 = 1.344$ and $a_2 = 0.043$, (fwhm, d, s in mm).

A second important aspect of the induction process is the sharing of the induced charge between anode and cathode electrodes. In fact, while the charge induced on the anode wires is essential for the functioning itself of a MWPC, on the other hand many read-out systems rely on the charge induced on the cathode wires or strips. To optimize the signal-to-noise ratio is, therefore, useful to know the fraction of the avalanche charge induced, at any time, on the cathodes in dependence of the particular choice of the geometrical parameters of a MWPC. Fig. 4a shows a fit of the calculated ratio as a function of s, with d as parameter, after $T = 100$ ns, while fig. 4b shows the same data as a function of d with s as a parameter. Similar relations can be obtained for each time, thus allowing an optimization of the integration

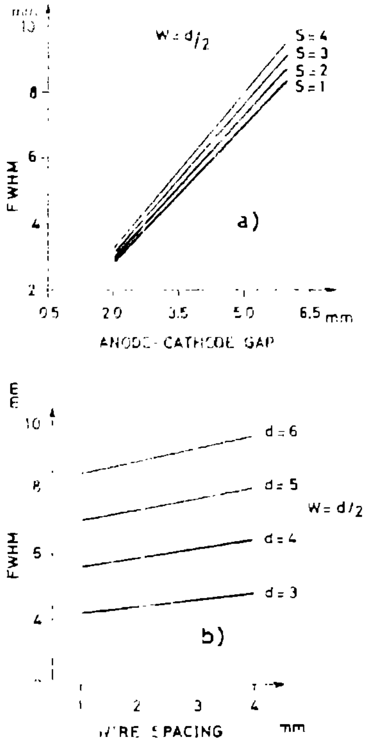

Fig. 3. (a) The width (fwhm) of the cathode charge distribution as a function of d with s as a parameter; (b) the same data as a function of s with d as a parameter; $w = d/2$ in all cases.

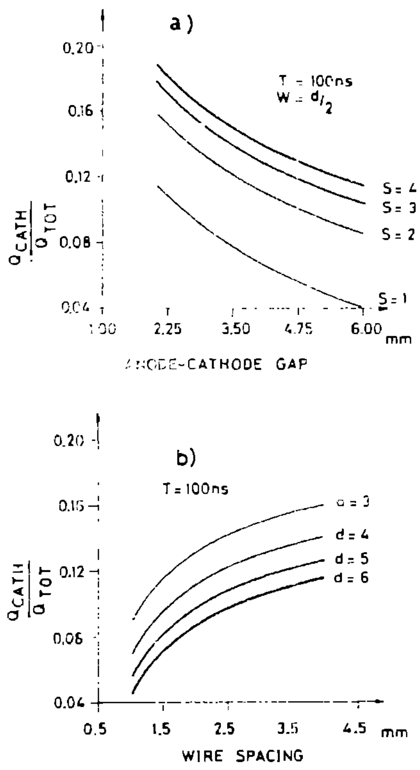

Fig. 4. (a) The fraction of cathode charge relative to the avalanche charge plotted as a function of d with s as a parameter; (b) the same data plotted as a function of s with d as a parameter.

and differentiation time constant of the read-out system. For instance, the fraction of charge on each cathode is 7% after 20 ns, 11% after 100 ns, slowly rising to 17% after 1 μs for a chamber with $d = 4$ mm and $s = 2$ mm.

Both these results, i.e. the distribution width and the overall cathode charge, were obtained for an avalanche with a uniform angular distribution and a constant size $Q = 10^7$ electrons. For each particular configuration the anode–cathode potential difference was then calculated to ensure a constant gas gain according to a slightly modified Rose and Korff model of avalanche growth [4]. The ion mobility was assumed to be $\mu = 1.2$ $cm^2V^{-1}s^{-1}$.

3. Integral and differential nonlinearity of position measurement

Most of the measurements of the avalanche position, especially in the direction parallel to the anode wires, are based on finding the centroid of the cathode charge distribution. The centroid can be determined by a global, continuous read-out employing delay-lines or, alternatively, by a direct computation from the individually measured strip charge [5]. In this latter case the problem arises of the optimum number of strips needed to accurately sample the distribution of the cathode signals. Too few sampling strips can result in a discontinuity or modulation in the position response function, while too many sampling electrodes greatly increase the electronics complexity or impair the S/N ratio [6]. To address this problem we have modelled the position response function, i.e. the calculated centroid versus the true position of the avalanche as a function of the width (w) of the cathode strips. As one can see from fig. 5, starting from $w > d$ the position response function is severely modulated with a period equal to w. The maximum absolute error (integral nonlinearity) which, in this case, is a function of the strip width only, can reach a value as large as 860 μm for $w = 2.5d$ and $d = 4$ mm. At

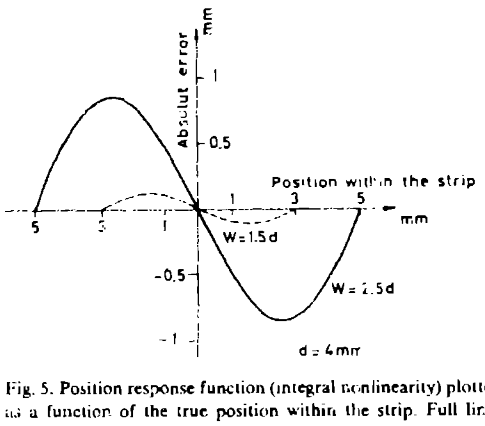

Fig. 5. Position response function (integral nonlinearity) plotted as a function of the true position within the strip. Full line: $w=2.5d$, dotted line: $w=1.5d$, $d=4$ mm, $s=2$ mm.

$w=1.5d$ the integral nonlinearity decreases to 25 μm. The differential nonlinearity, defined as the derivative of the integral nonlinearity, is a very sensitive measure of discontinuities or local artefacts in the position response function. A differential nonlinearity $>1\%$ can already be achieved at $w=d$ (fig. 6). A modulation effect of this type was experimentally measured by Radeka and Boie [5], by Chiba et al. [7] and Piuz et al. [8]. A compromise between accuracy and linearity and the number of sampling electrodes is therefore mandatory. However, for $w=d$ three or four strips are already sufficient to accurately sample the cathode distribution for a MWPC with $d=4$ mm and $s=2$ mm.

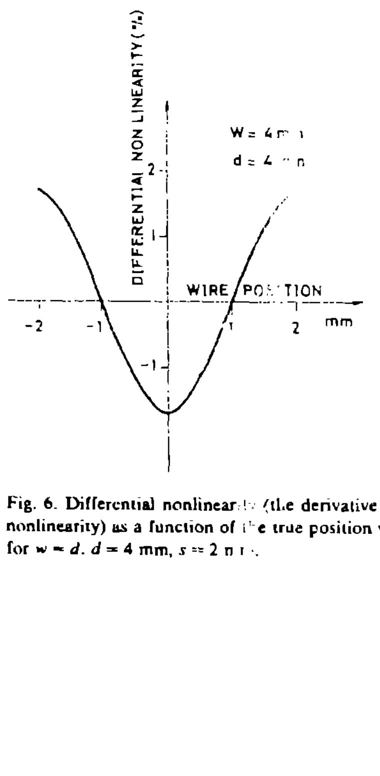

Fig. 6. Differential nonlinearity (the derivative of the integral nonlinearity) as a function of the true position within the strip for $w=d$, $d=4$ mm, $s=2$ mm.

4. Left–right and top–bottom ambiguity resolution and interpolation between anode wires

A well known problem in the operation of multiwire drift chambers is the left–right ambiguity, i.e. two tracks located at the same distance but on either side of the anode wire cannot be resolved [9]. However, several authors [9–11] have experimentally shown that this ambiguity can be resolved if the induced cathode signals are used to obtain the spatial information, provided that the gas gain is kept sufficiently low so that the avalanche does not surround the wire in a uniform way but, rather, exhibits an azimuthal asymmetry.

Fischer et al. [10] have shown that in the operating mode of proportional gas amplification the avalanche is well localized on the side of the anode wire where electrons arrive from the point of primary ionization and the shape of the avalanche is well reproduced by a Gaussian curve with a typical σ ranging from 30° to 45°.

We have studied the displacement of the reconstructed centroid of the cathode distribution as a function of the primary ionization collection angle for an avalanche of Gaussian shape and with a σ of 30°, after a time $T=20$ ns (fig. 7). The maximum displacement is, naturally, found for $\theta=0°$ and $\theta=180°$ where it reaches the value $\Delta X=\pm 120$ μm. It is worth noting that this result is in very good agreement with the experimental result obtained by Walenta [9] which used a fast delay-line read-out with 20 ns differentiation time constant. Since in the first 20 ns only the ionization clusters delivered at the shortest radial distance from the wire are collected, this ensures that the displacement effect will be observed whatever the track distance from the wire. Fig. 8 shows the centroid displacement as a func-

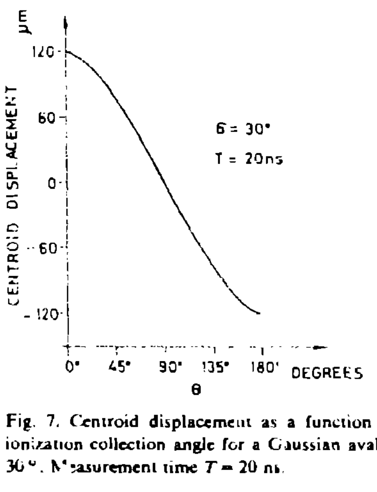

Fig. 7. Centroid displacement as a function of the primary ionization collection angle for a Gaussian avalanche with $\sigma=30°$. Measurement time $T=20$ ns.

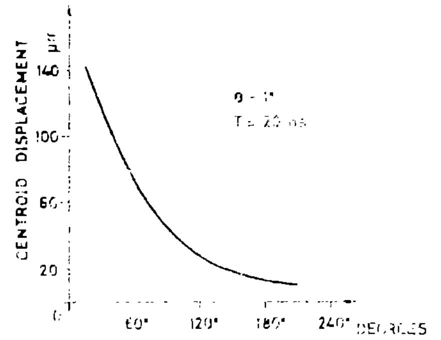

Fig. 8. Centroid displacement as a function of the width of a Gaussian avalanche for a collection angle $\theta = 1°$.

tion of σ, the width of the Gaussian distribution of the avalanche, for a collection angle θ of 1°. The narrower is the avalanche spreading, the larger the centroid displacement.

A further ambiguity exists in the operation of a MWPC as X or γ-ray detector: one does not know if the conversion process has occurred in the upper or lower half of the detector itself. This indetermination increases the parallax error, expecially for thick detectors such as those needed to capture high-energy gammas (positron tomography, X-ray crystallography, etc.). A solution to this problem can be found by taking advantage of the azimuthal asymmetry of the avalanche. Particularly useful will be the operation of the chamber in the "self-quenching streamer" mode. In this case the "streamer" is completely confined on the side of the wire where the multiplication process started. Since the signal is mainly due to the collection of the ionization electrons, the positive ions were substituted with "positive electrons" drifting toward the cathodes with a velocity V of 5 cm/μs. Fig 9a shows the resulting pulse-height for an avalanche centered at −90° which extends 1 mm from the anode wire and for a similar one centered, on the other side, at +90°. Fig. 9b shows the case of $\theta = +45°$ and $\theta = +225°$. The huge difference can be exploited [12] by sending the cathode signals picked up, for example, by a delay-line to a difference amplifier and looking at the polarity of the output signal.

An attractive characteristic of a MWPC operated at very low gas gain is the possibility of interpolation between anode wires, i.e. the possibility of reconstructing the true position of an ionization event which occurred between two different anode wires. A demonstration of this possibility was given by Charpak et al. [13], which showed a good quality MWPC image of an object whose height was less than the wire spacing. A qualitative explanation of this effect can be obtained when considering that if a positive ions cloud is allowed to drift backward for a long time along the same field line of collection of the primary ionization, the center of gravity of the induced charge will be progressively displaced from the anode wire toward the actual position of the primary event. This effect can be quantitatively addressed by studying the centroid displacement as a function of the drift time for an arbitrary θ. From fig. 10 we can see that after $T = 10$ μs the displacement effect begins to saturate, i.e. no further displacement can be obtained after this time. Fig. 11 shows that a good linear relationship exists between this displace-

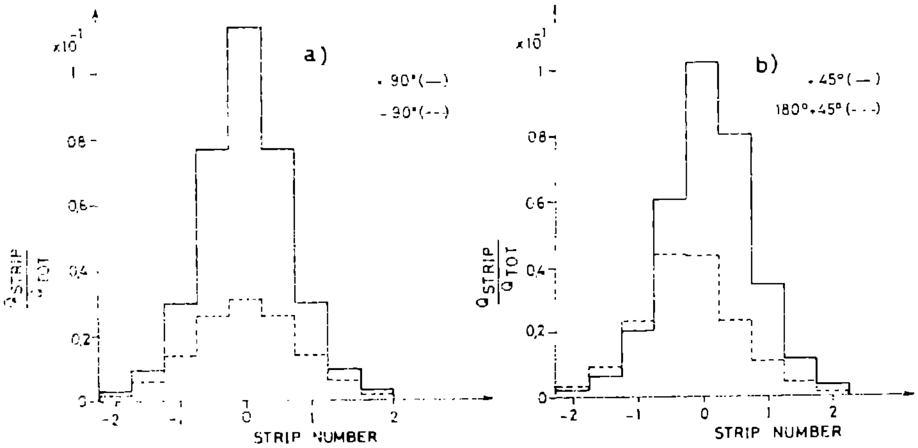

Fig. 9. (a) Cathode charge distributions for a "streamer" centered at +90° (full line) or −90° (dotted line), both extending 1 mm from the anode wire; (b) the case of $\theta = +45°$, $\theta = +225°$.

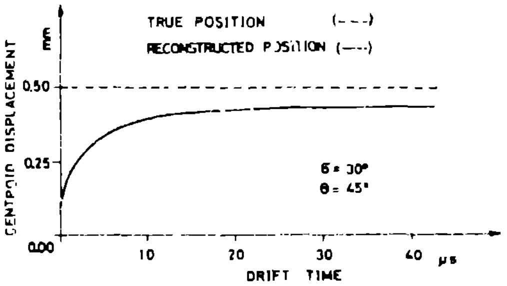

Fig. 10. Centroid displacement as a function of the measurement time T for a Gaussian avalanche with $\sigma = 30°$ and collection angle $\theta = 45°$ (full line). The dotted line represents the true position of the event.

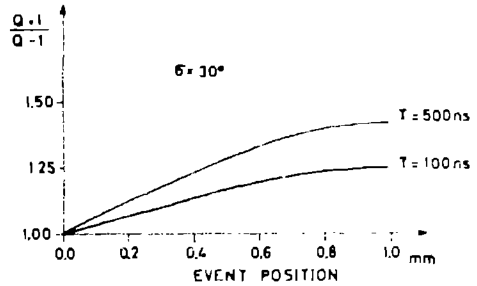

Fig. 12. The ratio Q^{+1}/Q^{-1} of the charge on the wires adjacent to the avalanche wire as a function of the true position of the event for a Gaussian avalanche with $\sigma = 30°$, after $T = 100$ ns (thick line) and after $T = 500$ ns (thin line).

ment and the true position of the primary event for a $\sigma = 30°$ and a measurement time $T = 20$ μs.

A more sensitive and fast measurement of the actual position of the event between two anode wires can be obtained by looking at the signals on the wires adjacent to the avalanche wire. Fig. 12 shows the ratio Q^{+1}/Q^{-1} as a function of the true position of the event for an avalanche with $\sigma = 30°$, after $T = 100$ ns (thick line) and $T = 500$ ns (thin line). A good linear relationship exists, especially in the case of the larger integration time.

5. The temporal and spatial behaviour of the signals from extended tracks

In this section we describe an improvement of the Erskine model to include extended or inclined tracks such as those produced by minimum ionizing particles. For a chamber with $d = 5$ mm and for perpendicular incidence the ionization track was transformed in a random distribution of 34 clusters. The coordinate l of

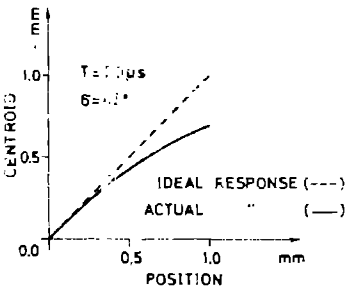

Fig. 11. Position response function for a point ionization with Gaussian angular distribution ($\sigma = 30°$). Measurement time $T = 20$ μs. Full line: reconstructed event position, dotted line: ideal response.

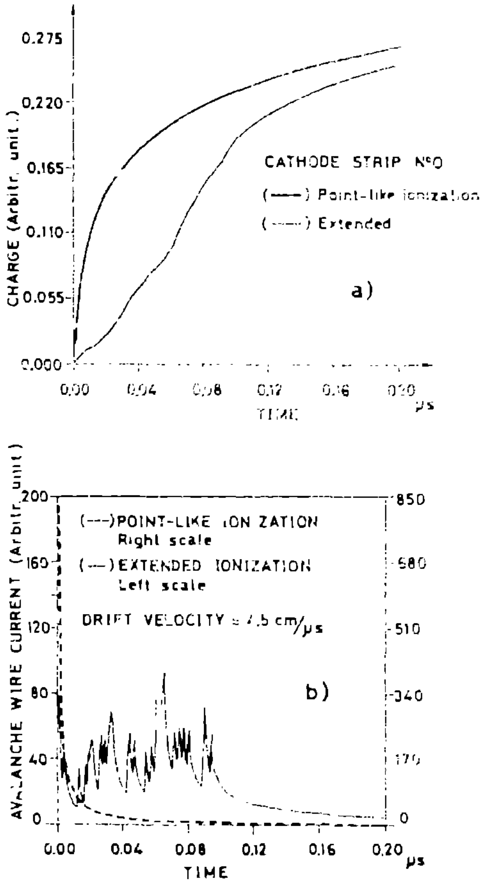

Fig. 13. (a) Time course of the cathode charge signal for point and extended ionization tracks; (b) the anode current signals. The time of arrival of each individual clusters is evident.

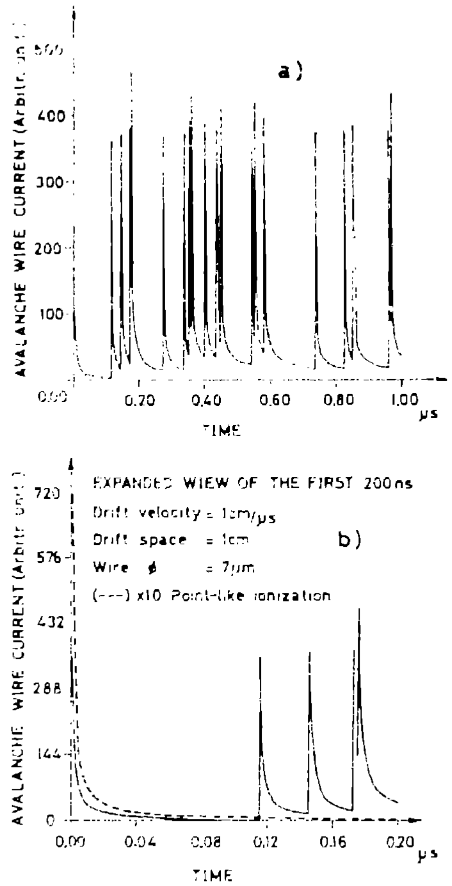

each cluster was derived with the Monte Carlo method [15] through the relation $l = -\lambda \ln(\xi)$ where ξ is a random number in the interval (0,1) extracted from a uniform distribution and λ is the particle mean-free-path. The contribution to the signal development of each individual cluster was computed and summed with the appropriate time lag to the previous one. The resulting time course of the charge and current signals is depicted in fig. 13 together with the corresponding signals from a point ionization source for the case of a normal gas mixture. The rise-time difference and the characteristic oscillation of the current signal are evident. This latter phenomenon is at the base of the cluster counting technique [14]. This technique aims to measure the differential energy loss of the incident charged particle by counting each individual cluster arriving at the anode wire. Since the distribution of the number of clusters is Poissonian, this technique should be superior to the measurement of the total ionization, which obeys the wider Landau distribution. A modelling of the current signal can then help in selecting the appropriate gas mixture, the electric field strength, the anode wire diameter and in designing the counting electronics chain. Fig. 14 shows the current signal developing on the anode wires of a "time expansion chamber" such as that proposed by Walenta [14]. A signal like that of fig. 14 poses severe constraints on the performance of the preamplifier which should have a very large band-width and a very low input impedance

Fig. 14. (a) A simulation of the current signal of a "time expansion chamber". The electron drift velocity is reduced to 1 cm/μs and dl/dx $n = 20$ clusters/cm; (b) expanded view.

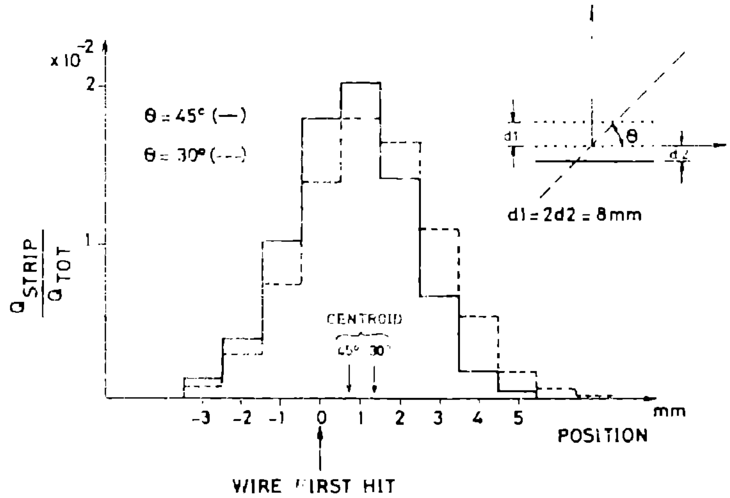

Fig. 15. Cathode charge distributions for two inclined tracks with $\theta = 30°$ and $\theta = 45°$. The upper half of the MWPC is two times thicker than the lower half. The arrows indicate the location of the wire first hit and the reconstructed centroid.

to effectively preserve the shape of the current signal.

A track making an angle θ with the direction orthogonal to the anode wires was modelled assuming that all the ionization clusters delivered within a particular field cell ($-s/2$, $+s/2$) drift toward the corresponding anode wire. The resulting cathode charge distribution (fig. 15) will be wider and flatter. If we now consider a highly asymmetric chamber with, for example, $d_1 = 2d_2$ and the potential on each cathode adjusted to have a radially symmetric field all around the anode wire, the top–bottom asymmetry in the collection and multiplication process will be reflected in a displacement of the charge centroid relative to the wire first hit. This displacement could then be used as an indicator of the angle of particle incidence. A delay-line read-out can be a useful mechanism of "amplification" of this effect. In fact, the one-half on the delay-line signal that is travelling in the direction where the ionization is still to be collected and multiplied, will receive a greater charge contribution relative to the second one-half. At the end of the delay-line will then appear signals which differ by amplitude as well as by shape. The most effective "amplification" will be observed when the specific delay of the delay-line matches the electron drift velocity. Fig. 16 shows an example of a simulation of this effect for a chamber with $d_1 = 2d_2 = 8$ mm, $s = 2$ mm, angles of incidence $\theta = 30°$ and $60°$, specific delay = 100 ns/cm, total delay = 200 ns. A pulse height difference as large as 50% could be observed in this case. This effect could be used as a sort of "electronic collimation", when imaging distributions of isotropically emitting sources.

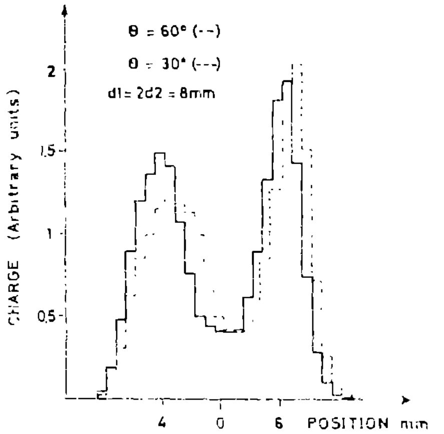

Fig. 16. The delay-line signals after 200 ns of delay for an inclined track with angle of incidence $\theta = 30°$ (full line) and $\theta = 60°$ (dotted line); $d = 4$ mm, $s = 2$ mm, specific delay = 100 ns/cm.

6. Conclusions

We have shown how the use of a mathematical model can be of great help in designing MWPC-based detection systems. The time and spatial behaviour of the signals coming from the detector can be completely predicted and the implications of any particular choice can be quantitatively analyzed. In this paper we have shown a practical example of this possibility, focussing our attention on few, but important items concurring to define the overall performance of a MWPC.

The Erskine formalism has been shown to be very suitable for this task, allowing a straightforward extension to ionization tracks like those released by minimum ionizing particles.

We thank Mr. E. Carboni for his careful drawing of the figures.

References

[1] G.A. Erskine, Nucl. Instr. and Meth. 198 (1982) 325.
[2] I. Endo et al., Nucl. Instr. and Meth. 188 (1981) 51.
[3] G. Fischer and J. Plch, Nucl. Instr. and Meth. 100 (1972) 515.
[4] V. Palladino and B. Sadoulet, Nucl. Instr. and Meth. 128 (1975) 323.
[5] V. Radeka and R.A. Boie, Nucl. Instr. and Meth. 178 (1980) 543.
[6] E. Gatti et al., Nucl. Instr. and Meth. (1979) 83.
[7] J. Chiba et al., Nucl. Instr. and Meth. 206 (1983) 451.
[8] P. Piuz et al. Nucl. Instr. and Meth. 196 (1982) 451.
[9] A.H. Walenta, Nucl. Instr. and Meth. 151 (1978) 461.
[10] J. Fischer et al., Nucl. Instr. and Meth. 151 (1978) 451.
[11] G. Charpak and F. Sauli, CERN Report 73-4 (1973).
[12] A. Del Guerra et al., IEEE Trans. Nucl. Sci. NS-30 (1983) 646.
[13] G. Charpak et al., Nucl. Instr. and Meth. 148 (1978) 471.
[14] A.H. Walenta, IEEE Trans. Nucl. Sci. NS-26 (1979) 73.
[15] F. Lapique and F. Piuz, Nucl. Instr. and Meth. 175 (1980) 297.